Potential and Performance of Anisotropic 19F NMR for the Enantiomeric Analysis of Fluorinated Chiral Active Pharmaceutical Ingredients

Boris Gouilleux, François-Marie Moussallieh, Philippe Lesot

Analyst

PAPER

View Article Online
View Journal

Cite this: DOI: 10.1039/d4an00237g

Potential and performance of anisotropic ^{19}F NMR for the enantiomeric analysis of fluorinated chiral active pharmaceutical ingredients†

Boris Gouilleux, *[a] François-Marie Moussallieh [a] and Philippe Lesot *[a,b]

Controlling the enantiomeric purity of chiral drugs is of paramount importance in pharmaceutical chemistry. Isotropic ^{1}H NMR spectroscopy involving chiral agents is a widely used method for discriminating enantiomers and quantifying their relative proportions. However, the relatively weak spectral separation of enantiomers (^{1}H $\Delta\delta_{iso}(R, S)$) in frequency units at low and moderate magnetic fields, as well as the lack of versatility of a majority of those agents with respect to different chemical functions, may limit the general use of this approach. In this article, we investigate the analytical potential of ^{19}F NMR in anisotropic chiral media for the enantiomeric analysis of fluorinated active pharmaceutical ingredients (API) *via* two residual anisotropic NMR interactions: the chemical shift anisotropy (^{19}F-RCSA) and dipolar coupling ((^{19}F–^{19}F)-RDC). Lyotropic chiral liquid crystals (CLC) based on poly-γ-benzyl-L-glutamate (PBLG) show an interesting versatility and adaptability to enantiodiscrimination as illustrated for two chiral drugs, Flurbiprofen® (FLU) and Efavirenz® (EFA), which have very different chemical functions. The approach has been tested on a routine 300 MHz NMR spectrometer equipped with a standard probe (5 mm BBFO probe) in a high-throughput context (*i.e.*, ≈10 s of NMR experiments) while the performance for enantiomeric excess (*ee*) measurement is evaluated in terms of trueness and precision. The limits of detection (LOD) determined were 0.17 and 0.16 μmol ml^{-1} for FLU and EFA, respectively, allow working in dilute conditions even with such a short experimental duration. The enantiodiscrimination capabilities are also discussed with respect to experimental features such as CLC composition and temperature.

Received 12th February 2024,
Accepted 16th April 2024

DOI: 10.1039/d4an00237g

rsc.li/analyst

Introduction

Molecular chirality plays a central role in pharmaceutical chemistry as more than 50% of the drugs currently sold on the market include at least one stereogenic center.[1] While one of the enantiomers of a chiral active pharmaceutical ingredient (API) leads to the expected/desired activity on the biological target (eutomer), the other one may induce different effects, ranging from no activity to opposite or even toxic side-effects (distomer).[1–3] As a result, an increasing number of new chiral drugs are being marketed as pure enantiomeric compounds, while some drugs initially used as a racemate are being replaced by the identified eutomer (chiral switch) to improve therapeutic activity/efficacy.[4] This leads to a continued need for fast, efficient and versatile analytical tools to determine the enantiomeric purity of a bioactive substance at various stages, from drug synthesis steps to the control of the final commercial medicines.

Several approaches have been developed for enantiomeric discrimination and the determination of enantiomeric excess (*ee*), so far, such as chiroptical tools (VCD, ROA, ...), gas or liquid chiral chromatography (GC, HPLC), electrophoresis, mass spectrometry and NMR spectroscopy.[5] Although chromatographic tools are widely used for this purpose, NMR spectroscopy can also be successfully used for the enantiomeric analysis of chiral API.[6–13] These NMR methods rely on the interaction between the analyte to be studied and a chiral auxiliary (CA) to form: (i) either stable diastereoisomers by covalent bonding or (ii) diastereomeric adducts *via* intermolecular interaction.[14–16] In isotropic solutions, these CAs can be either chiral derivatizing agents (CDAs) as Mosher's acid,[17] chiral metallic complexes,[18,19] chiral lanthanide shift reagents,[20,21] or chiral solvating agents (CSAs) such as cyclodextrin-based agents.[22] The conversion of enantiomers to diastereomeric entities leads to spectral discriminations through variations of isotropic chemical shift ($\Delta\delta_{iso}(R, S)$).

[a]Université Paris-Saclay, UFR d'Orsay, RMN en Milieu Orienté, ICMMO, UMR CNRS 8182, Bât. HM1, 17-19, Avenue des Sciences, 91400 Orsay, France
[b]Centre National de la Recherche Scientifique (CNRS), 3, Rue Michel Ange, F-75016 Paris, France. E-mail: boris.gouilleux@universite-paris-saclay.fr, philippe.lesot@universite-paris-saclay.fr

†Electronic supplementary information (ESI) available: (i) NMR sample composition, *ee*(%) and uncertainty; (ii) assignment of ^{13}C–^{19}F satellites on ^{19}F–{^{1}H} spectra of FLU in PBLG/$CHCl_3$; (iii) further ^{19}F–{^{1}H} spectra of EFA at different *ee*% or temperature; (v) limits of detection (LOD). See DOI: https://doi.org/10.1039/d4an00237g

Basically, weak spectral enantio-separations (in frequency units) generally measured on routine ^{1}H NMR (<9.4 T) can be increased by recording spectra on very high-field NMR instruments (if accessible). Other approaches using ^{19}F NMR on fluorinated solutes[23] or even fluorinated CSA/CDA as recently reported,[24–27] can provide elegant tools. However, the need of designing a tailored CSA/CDA (not always commercially available) for a specific chemical group remains the main challenge and may limit the general use of these approaches.

The concept of enantiospecific non-covalent interactions between the *R*/*S*-isomers and a chiral (enantiopure) selector in isotropic solvents can be extended to anisotropic media, such as chiral weakly aligning systems (*e.g.*, helical polymer-based lyotropic liquid crystals). In this case, enantiomers exhibit a difference of orientational order in average, these molecular orientations being generally expressed by the Saupe tensor $S_{\alpha\beta}$.[28] From NMR point of view, the spectral enantiomeric discriminations are observed through a difference of residual anisotropic NMR interactions, such as residual chemical shift anisotropy (RCSA), residual dipolar coupling (RDC) or residual quadrupolar coupling (RQC), whose amplitudes depend on the orientational order of the analyte.[29–34]

Compared to NMR methods in isotropic solvents supported by CAs, NMR in chiral weakly aligning media offers at least three analytical advantages that can expand the role of NMR spectroscopy in chiral analysis of chiral drugs. The first and the most interesting one is the diversity and the magnitude of these anisotropic observables (RDC, RQC, RCSA) associated with any magnetically active nucleus (whether abundant or not), and that generally allows for effective spectral enantiodiscriminations. In addition, the magnitude of RQCs and RDCs (unlike a chemical shift difference) is independent of the magnetic field strength (B_0), making easier to transfer methods to spectrometers operating at lower fields. The second one results from the shape recognition mechanisms that play a central role in enantiodiscrimination mechanisms in CLCs.[35] As a result, no specific chemical functions or group on the analyte (unlike CSAs/CDAs) is required, so that all CLCs are potentially able to differentiate enantiomers whatever the chemical characteristics of the chiral analyte. The third advantage is based on the absence of possible differences in affinity between the analyte and the chiral agent which can lead to significant discrepancies between the real value and the measured value of the *ee*%.[24,27] *De facto*, no correction coefficient must be introduced to determine the *ee*% from the measurement of peak surfaces for each enantiomer. The last but not the least advantage is that several chiral polymers (as polypeptides) are commercially available, and no preliminary synthetical step is required to explore their potential.

Although these properties have benefited organic chemistry for the analysis of small molecules, NMR in CLCs has been little explored for the study of pharmaceutical compounds, so far. The main reason for this lack of interest is the inherent complexity of anisotropy ^{1}H 1D NMR spectra of medium-sized molecules due to the numerous long-range (^{1}H–^{1}H)-RDCs that broaden spectral patterns. Other exploitable heteronuclear experiments (*e.g.*, ^{13}C and ^{2}H) are possible but may suffer from insufficient sensitivity to deal with samples of 5–20 mg of API at high enantiomeric excess in a high-throughput framework with routine NMR equipment (*e.g.*, 300–400 MHz spectrometers and conventional probes). In this context, ^{19}F–{^{1}H} NMR appears to be a promising alternative since in the case of monofluorinated or trifluoromethylated chiral compounds (F-R* or CF_3-R*) encountered in pharmacopeia,[36] a dramatic simplification in spectral analysis is expected, with a suitable/reasonable sensitivity (≈86% of ^{1}H NMR) and a significant chemical shift dispersion of ^{19}F resonances. This advantage has recently been exploited for the chiral analysis in isotropic solvents involving either fluorinated analytes (or even a mixture of chiral analytes),[7,23] or newly developed chiral agents including a fluorine tag.[24–26]

From anisotropic NMR point of view, ^{19}F nuclei are rather sensitive nuclear spies to observe molecular orientational order differences induced by weakly chiral oriented media. These differences can be observed through two residual anisotropic interactions for *R* and *S* isomers: the ^{19}F-RCSA, also noted, ^{19}F $\sigma_{\text{aniso}}(R, S)$, and the (^{19}F–^{19}F)-RDC, noted $|D_{\text{FF}}(R, S)|$. Based on ^{19}F-RCSA, the spectral enantiomeric discrimination is measured through a difference of frequency (in Hz or ppm) between each enantiomer:

$$|\Delta\nu_{\text{aniso}}(R,S)| = |\nu_{\text{aniso}}(R) - \nu_{\text{aniso}}(S)| \quad (1)$$

where

$$\nu_{\text{aniso}}(R,S) = -\frac{\gamma_{\text{F}}}{2\pi}(1 - \sigma_{\text{iso}} - \sigma_{\text{aniso}}(R,S))B_0 \quad (2)$$

Expressed in a molecular frame (*a*, *b*, *c* axes), the terms σ_{iso} and σ_{aniso} can be derived from the shielding tensor as:

$$\sigma_{\text{iso}} = \frac{1}{3}(\sigma_{aa} + \sigma_{bb} + \sigma_{cc})$$

and

$$\sigma_{\text{aniso}} = \frac{2}{3}\sum_{\alpha,\beta=a,b,c}\sigma_{\alpha\beta}S_{\alpha\beta} \quad (3)$$

In the above equations ν and σ are related to the ^{19}F nuclei while γ_{F} is the fluorine gyromagnetic ratio.

Based on (^{19}F–^{19}F)-RDC, the spectral discrimination between enantiomers is measured as:

$$|\Delta D_{\text{FF}}(R,S)| = |D_{\text{FF}}(R) - D_{\text{FF}}(S)| \quad (4)$$

where

$$D_{\text{FF}} = -k_{\text{FF}}\frac{S_{\text{FF}}}{r_{\text{FF}}^3} \quad (5)$$

The order parameter S_{FF} of the internuclear vector r_{FF} between the coupled ^{19}F nuclei can be derived as:

$$S_{\text{FF}} = \sum_{\alpha,\beta=a,b,c}\cos\theta_{\text{FF}}^{\alpha}\cos\theta_{\text{FF}}^{\beta}S_{\alpha\beta} \quad (6)$$

In eqn (3) and (6), $S_{\alpha\beta}$ is the Saupe order matrix, a 2nd rank tensor, describing the orientational order of a solute in an (*a*, *b*, *c*) axis system attached to the molecule.

Previous analysis of around twenty small fluorinated chiral compounds (monofluorinated or including a $-CF_3$ moiety) using poly-γ-benzyl-L-glutamate (PBLG) as a chiral mesophase has shown that variations in the ^{19}F anisotropic chemical shift and ^{19}F–^{19}F total homonuclear coupling lie in a range from 0.01 to 0.350 ppm and from 1.4 to 118 Hz, respectively.[37–39] Based on this valuable enantiodiscrimination ability, we investigate for the first time the analytical potential of this approach to determine enantiomeric excesses (*ee*) for fluorinated chiral pharmaceutical ingredients using a routine 300 MHz (7.05 T) spectrometer equipped with a conventional 5 mm NMR probe, a commonly encountered setup in both academic and industrial laboratories. The key role of the mesophase composition and temperature on the enantiomeric resolution is investigated and presented in detail. The analytical performance of the herein method is then evaluated in terms of precision (here short-term repeatability), trueness (*i.e.*, deviation from the expected *ee*% values) and limits of detection. Two different APIs are targeted in this study: (i) Flurbiprofen® (**FLU**), a chiral non-steroidal anti-inflammatory drug where the (*S*)-form possesses most of the beneficial anti-inflammatory activity,[40] and (ii) Efavirenz® (**EFA**), a chiral drug whose (*S*)-isomer is a non-nucleoside inhibitor of human immunodeficiency virus (HIV) reverse transcriptase (see Scheme 1).[41] These two bioactive chiral molecules involve various chemical functions: **FLU** is a biphenyl propionic carboxylic acid while **EFA** is mainly characterized by a carbamate function into a benzoxazine ring, as well as a difference of fluorine moiety: a single fluorine in **FLU** *versus* a trifluoromethyl group ($-CF_3$) in **EFA**. In addition, the fluorinated group used for the enantiomeric discrimination is directly bound to the stereogenic center in **EFA** whereas the latter is located further away in the case of **FLU**. Interestingly, while **EFA** undergoes restricted degrees of freedom, **FLU** is a more flexible molecule which can experience conformational changes upon interaction with PBLG side chains.[42] This may lead to different chiral recognition mechanisms between these two APIs with respect to the CLC. From an analytical point of view, all these chemical characteristic differences make **FLU** and **EFA** very well-suited analytes to test the versatility of PBLG mesophase when applied to the analysis of pharmaceutical compounds.

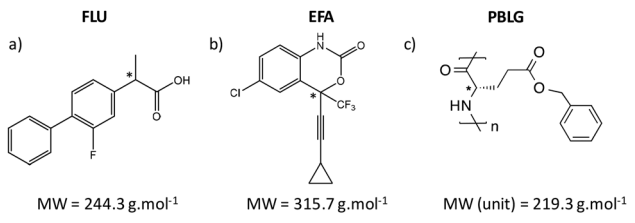

Scheme 1 Molecular structures of (a) Flurbiprofen® (**FLU**) and (b) Efavrienz® (**EFA**) and (c) PBLG polymer, along with the molecular weights (MW). The star indicates the position of the stereogenic center in each structure.

Experimental

Chemicals and preparation of oriented samples

(*R*)-Flurbiprofen was purchased at Acros Organics with a purity of 97%. *rac*-Flurbiprofen was purchased at Sigma-Aldrich (Merck) with a purity of 98%. (*S*)-Efavirenz was purchased at TCI with a purity of 98%. *rac*-Efavirenz was purchased at Toronto Research Chemical (TRC) with a purity of 97%. The PBLG polymer (Lot SLBZ3570 with a degree of polymerization DP = 849) was purchased at Aldrich (Merck). All compounds were used with any further purification.

The oriented samples were prepared directly in the NMR tube by mixing the chiral analyte (<30 mg), the PBLG (nearby 100 mg) and the organic co-solvent ($CHCl_3$). The amount of chloroform (about 600 mg) was here adjusted so that the total weight% of PBLG (*i.e.*, mass of PBLG/total mass) was maintained at around 14%, and the sample length reached 4 cm. The exact sample compositions are given in Table SI-1 in ESI.† The 5 mm NMR tube was then fire-sealed to avoid $CHCl_3$ evaporation over time and several low-speed centrifugation cycles of the sample (*e.g.*, 500 rpm during 20 s) were carried out to remove matter gradients. The tube was inverted between each centrifugation.

NMR equipment and experiments

^{19}F NMR experiments were performed on a 7.05 T ($\nu_0(^{19}F)$ = 282.4 MHz) Bruker NEO spectrometer equipped with a 5 mm BBFO probe or on a 9.4 T ($\nu_0(^{19}F)$ = 376.5 MHz) Bruker AV1 spectrometer equipped with a 5 mm QXO probe. As this probe is not tunable for the ^{19}F emission–reception, resulting in a significant sensitivity penalty, the analytical performance for the *ee*% determination was evaluated at 7.1 T with the BBFO probe.^{19}F–$\{^1H\}$ NMR spectra were recorded with a 90° radiofrequency pulse of 15 μs at 282.4 MHz and of 111 μs at 376.4 MHz, and the classical WALTZ-16 sequence was used as ^1H composite pulse decoupling. Free induction decay (FID) was sampled during 0.85 s and 0.55 s for **FLU** and **EFA** samples, respectively. The inter-scan delay was adjusted to reach a repetition time $T_R \sim 1.25 \times T_1$ (^{19}F) for optimal signal-to-noise-ratio (SNR) per time unit. Given the short experimental duration (*e.g.*, 10 s), ^{19}F–$\{^1H\}$ spectra are not impacted by the natural B_0 field drift, and hence all experiments were carried out in the absence of deuterium lock. Shimming procedure was performed manually or using an automatic shimming procedure on the ^1H signal of chloroform to optimize the signal line-shape. The achievement of this last step highly depends on the spatial uniformity of the liquid-crystalline phase.[43] The recorded FIDs are then processed on Mnova 14.2 (Mestrelab, Spain) including zero-filling (128k datapoints), filtering window, Fourier Transform, manual phasing and a polynomial (order 5) baseline correction. Specific experimental

parameters and processing details are directly indicated in each figure caption.

Measurement of the enantiomeric excess and line-fitting procedure

The enantiomeric excess (*ee*) is experimentally determined as:

$$ee(i) = \frac{A_i - A_j}{A_i + A_j} \quad (7)$$

where the subscript "*i*" refers to the enantiomer in excess (major isomer) and *A* is the peak surface. In practice, the signal integration was achieved by a line-fitting procedure provided by Mnova 14.2 software (Mestrelab, Spain) to reduce area bias in cases of enantiomeric signals non-fully baseline separated. This line-fitting procedure fits NMR lines with a linear combination of Lorentzian and Gaussian functions and finely tunes the height, the linewidth and the Lorentzian/Gaussian ratio. The linewidth and the Lorentzian/Gaussian ratio were not imposed constant for all the components of a same multiplet in order to take account of any slight asymmetry due to imperfect uniformity of the mesophase.

Results and discussion

^{19}F {^{1}H} NMR spectra of FLU and EFA in weakly chiral oriented media

In any oriented media, monofluorinated compounds as **FLU** give rise only to a singlet centred on ^{19}F δ_{aniso} on the ^{1}H-decoupled ^{19}F NMR spectrum, while the trifluoromethyl group (–CF_3) of **EFA** leads to a triplet (1 : 2 : 1) centred on ^{19}F δ_{aniso}. The splitting between lines is equal to $T_{FF} = 3D_{FF}$, due to the geminal ^{19}F–^{19}F residual dipolar coupling, noted (^{19}F–^{19}F)-RDC or D_{FF}, between the three homotopic ^{19}F nuclei (see Fig. 1b). The herein notation T_{FF} corresponds to the ^{19}F homonuclear total spin–spin coupling constant including only a dipolar contribution here. Note that in case of two diastereotopic (anisochronous) fluorine nuclei, the splitting observed for each doublet is equal to $T_{FF} = J_{FF} + 2D_{FF}$. In case of coupled fluorine nuclei in polyfluorinated molecules, enantiomers can be thus discriminated by a difference of ^{19}F $\delta_{aniso}(R, S)$, a variation of residual dipolar coupling: $\Delta T_{FF}(R, S)$ or a combination of both.

The former situation is observed on a racemic sample of **FLU** (see Fig. 2a) where the signals of enantiomers are separated by a difference of chemical shift anisotropy: ^{19}F $|\Delta\delta_{aniso}(R, S)|$ = 0.051 ppm, while the (*R*)- and (*S*)-isomers of a racemic sample of **EFA** are discriminated by variations of ^{19}F-RCSA: ^{19}F $|\Delta\delta_{aniso}(R, S)|$ = 0.085 ppm and (^{19}F–^{19}F)-RDC: $|\Delta T_{FF}(R, S)|$ = 12.1 Hz as shown in Fig. 2b. The linewidth is of the order of 2–3 Hz at half-maximum in these spectra, which underlines the satisfactory resolution obtained in such lyotropic CLCs. Note the weak lines marked by black stars in Fig. 2a do not arise from fluorinated impurities, but rather to satellite lines owing to short and long-range (^{13}C–^{19}F)-RDCs. Assignment of these signals to the multiple ^{13}C-isotopomers is detailed in ESI-III.†

Study of parameters affecting the spectral enantiomeric discrimination

Effects of mesophase composition. Polymeric-based lyotropic mesophases are ternary systems consisting of the homopolypeptide (*e.g.*, PBLG), the co-solvent (*e.g.*, $CHCl_3$) and the chiral solute (in racemic, scalemic or enantiopure series) to be analysed. Their relative (molar) proportions affect the amplitude of the anisotropic observables, and thus on the ability to discriminate between enantiomers. It is well-known that a high percentage of polymer increases the degree of order and therefore the amplitude of measured anisotropic observables. However, this advantage comes with a higher viscosity, which can lead to undesirable line broadening. In practice, ~14% of PBLG (weight% of the total mass) offers an interesting compromise and this value will be maintained in this work.

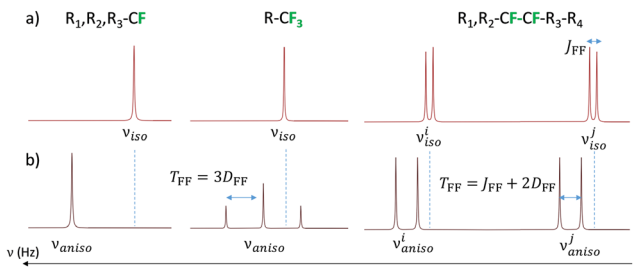

Fig. 1 Schematic description of ^{19}F spectral patterns expected to be observed by ^{19}F NMR in isotropic (a) and anisotropic media (b): (left) case of an isolated fluorine nucleus; (middle) case of three homotopic nuclei as met in a trifluoromethyl group; (right) case of two diastereotopic fluorine nuclei. Note the difference to spin–spin total coupling, T_{FF}, between homotopic (middle) and diastereotopic atom (right). Here is considered a deshielded effect of ^{19}F resonances (of various magnitudes) due to ^{19}F-RCSA. In case of a chiral solute dissolved in chiral oriented systems, a doubling of resonances (in the simplest case) is expected to be observed. The vertical scale is common to both isotropic and anisotropic media in the three cases (left, middle and right).

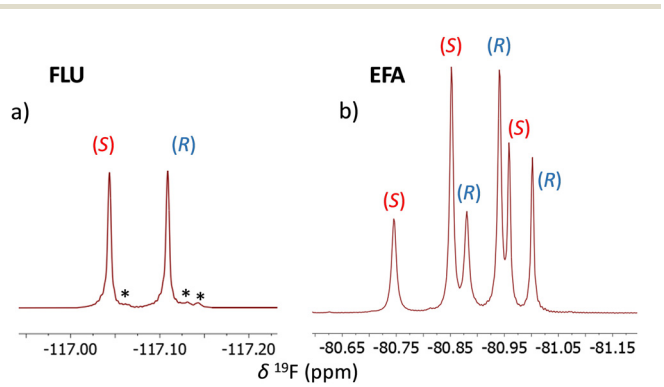

Fig. 2 282.4 MHz ^{19}F–{^{1}H} NMR spectra on 20 mg of racemic FLU (a) and EFA (b) dissolved in a PBLG/$CHCl_3$ based lyotropic liquid crystal. The assignment of the stereodescriptors *R* and *S* relies on further experiments performed on scalemic samples. The black stars at the bottom of NMR lines correspond to ^{13}C–^{19}F satellite lines (see details in ESI-III†).

The potential role of the analyte concentration on the resulting values of ^{19}F-RCSA and (^{19}F–^{19}F)-RDC has been little investigated so far, since it is generally considered as a guest molecule with minor impacts on the orienting properties of the mesophase. To explore this effect, anisotropic ^{19}F–{^{1}H} NMR experiments are carried out on a series of samples with a growing amount of (*S*)-**EFA** from 5.8 mg (0.046 mol L^{-1}) to 30.3 mg (0.24 mol L^{-1}), while the mass percentage of PBLG is kept constant nearby 14% (see Table SI-1†). The spectra of Fig. 3 show a large increase of both ^{19}F-RSCA and (^{19}F–^{19}F)-RDC as the concentration in (*S*)-**EFA** decreases. Besides, the offset from the ^{19}F δ_{iso} value varies from 0.080 to 0.560 ppm (*i.e.*, +600%), while $|T_{FF}|$ increases from 13.9 to 131.7 Hz (*i.e.*, +847%). Such a large variation in RDC quantities is not calculated for the co-solvent $CHCl_3$, whose the associated total coupling $|T_{CH}|$ only varies from 309 to 315 Hz (*i.e.*, 1.9% variation) for samples from 0.16 to 0.045 mol L^{-1} in **EFA**, which rules out a destabilization of the mesophase with the increasing amount of solute. In addition, analysis of ^{1}H self-diffusion experiments (^{1}H DOSY NMR)[44,45] under isotropic conditions has also precluded any possibility of concentration-dependent self-aggregation leading to a conformational change in **EFA**. Details are given in ESI-VII.†

Two arguments can be put forward to explain the variation in (^{19}F–^{19}F)-RDC in methyl group by simply considering the order parameter associated with the C–CF_3 vector:

$$S_{C-CF_3} = \frac{1}{2}\left\langle 3\cos^2\theta^{B_0}_{C-CF_3} - 1\right\rangle \quad (8)$$

(i) A change of S_{C-CF_3} induced by a reorientation of the C–CF_3 axis of the solute with a subsequent modification of the angle $\theta^{B_0}_{C-CF_3}$ between the C–CF_3 vector and the magnetic field B_0. This can lead to a significant increase of RDC, especially if $\theta^{B_0}_{C-CF_3}$ is initially closed to the magic angle (*i.e.*, 54.7°), (ii) a modification of the ensemble average ⟨...⟩ as a function of the solute concentration. This ensemble average can be seen, in a first approximation, as a fast exchanging system where:

$$\langle S_{C-CF_3}\rangle = p_b\left\langle S^{b}_{C-CF_3}\right\rangle + p_f\left\langle S^{f}_{C-CF_3}\right\rangle \quad (9)$$

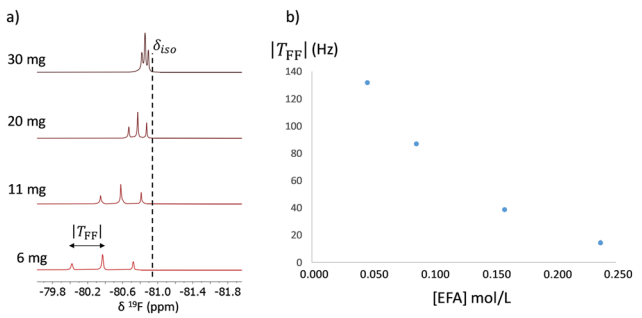

Fig. 3 (a) Series of ^{19}F–{^{1}H} NMR spectra recorded at 376.5 MHz with various amounts of (*S*)-EFA while the PBLG total weight% remains fixed at around 14%. The vertical dashed line indicates the ^{19}F chemical shift of the $-CF_3$ group in isotropic condition (*i.e.*, in $CDCl_3$). (b) Variation of $|T_{FF}|$ as a function of the concentration in EFA.

with p_b the fraction of oriented solutes $\left(\langle S^{b}_{C-CF_3} \neq 0\rangle\right)$ interacting with the chiral polymer and p_f the fraction of free solute ($p_b + p_f = 1$) in the co-solvent with a negligible orientational order $\langle S^{f}_{C-CF_3}\rangle$. Whenever the polymer interacting sites are saturated, an increase in solute concentration would lead to a smaller fraction p_b of solutes in the vicinity of the polymer chains and therefore to lower values of anisotropic observables. A combination of both effects could thus explain the observed variation in (^{19}F–^{19}F)-RDC while their relative contributions cannot be determined at this level.

In a second step, it is interesting to investigate the impact of the solute concentration when the two enantiomers are present in the chiral liquid crystal. At first, ^{19}F–{^{1}H} NMR experiments are performed on a series of racemic samples prepared with various amounts of **FLU**, from 4.8 to 30.0 mg, corresponding to a 0.025–0.153 mol L^{-1} concentration range for each enantiomer. Table 1 shows clearly the effect of solute concentration on the enantiomeric discrimination with an increase of ^{19}F $|\Delta\delta_{aniso}(R, S)|$ from 0.040 to 0.072 ppm for the highest and lowest concentration, respectively. In this case, diluted samples lead to a better spectral separation, which is an interesting analytical feature as the sensitivity of ^{19}F NMR enables experiments at relatively low concentrations. Furthermore, ^{19}F–{^{1}H} spectra are recorded on three different scalemic samples (*ee*(*R*) = 9.6, 58.2 and 88.7%) prepared with a fixed total amount of **FLU** (*i.e.*, 30 mg). As seen in Table 1, the variation of ^{19}F-RCSA progressively increases as a function of the enantiomeric excess: ^{19}F $|\Delta\delta_{aniso}(R, S)|$ = 0.054 ppm for *ee*(*R*) = 9.6% and 0.082 ppm for *ee*(*R*) = 89.5%. This effect of the enantiomeric excess on the resulting ^{19}F–{^{1}H} spectra is also visible for **EFA** as pointed out in Fig. SI-3† where in one hand ^{19}F $|\Delta\delta_{aniso}(R, S)|$ = 0.095 ppm and $|\Delta T_{FF}(R, S)|$ = 7.8 Hz for *ee*(*S*) = 71.5%, while ^{19}F $|\Delta\delta_{aniso}(R, S)|$ = 0.109 ppm and $|\Delta T_{FF}(R, S)|$ = 4.8 Hz for *ee*(*S*) = 90.5% in another hand.

Effects of temperature. In addition to the mesophase composition, the effect of temperature on the resulting ^{19}F–{^{1}H} spectra is evaluated. A slight linear decrease of ^{19}F $|\Delta\delta_{aniso}(R, S)|$ values is observed (R^2 = 0.9984) as a function of sample temperature in the case of a racemic sample (30 mg) of **FLU** (see Fig. 4), from ^{19}F $|\Delta\delta_{aniso}(R, S)|$ = 0.040 ppm at 297 K to

Table 1 Variation ^{19}F-RCSA values *versus* the amount of FLU and the associated enantiomeric excess[b]

m(FLU)[a] (mg)	*ee*(*R*) (%)	^{19}F $\|\Delta\delta_{aniso}(R, S)\|$ (ppm)
30.0	0.0	0.0403
20.2	0.0	0.0507
14.8	0.0	0.0549
10.2	0.0	0.0706
4.8	0.0	0.0720
30.0	0.0	0.0403
29.9	9.6	0.0543
30.8	58.2	0.0670
30.4	88.7	0.0820

[a] Total mass of FLU: *m*(*R*-FLU) + *m*(*S*-FLU). [b] All experiments were carried out with 14% (wt) of PBLG and at 297 K.

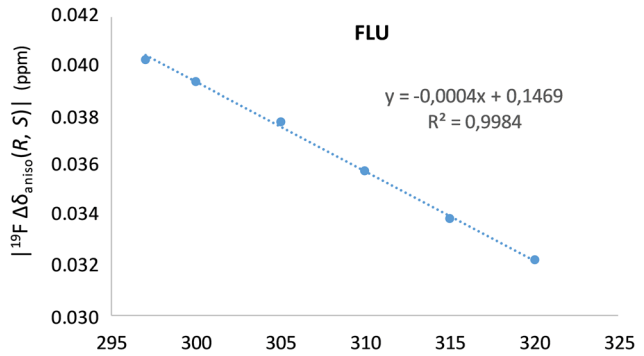

Fig. 4 Effect of the temperature on the enantiomeric discrimination by variation of ^{19}F-RCSA evaluated on a 30 mg racemic sample of FLU dissolved in PBLG/$CHCl_3$.

$|\Delta\delta_{aniso}(R, S)|$ = 0.032 ppm at 320 K. For a racemic sample of **EFA**, both ^{19}F δ_{aniso} and T_{FF} increase linearly *vs.* temperature for the two enantiomers. As the slopes of these linear variations are similar between enantiomers, ^{19}F $|\Delta\delta_{aniso}(R, S)|$ and $|\Delta T_{FF}(R, S)|$ remain constants at around 0.087 ppm and 13.0 Hz (see Fig. 5). However, these two anisotropic measurements vary at different rates in frequency units, resulting in distinct spectral patterns (see examples in Fig. SI-4†). Consequently, although the sample temperature does not influence the variation of ^{19}F δ_{aniso} and T_{FF} between enantiomers, this parameter should be adjusted to avoid potential peak-overlaps and thus facilitating the subsequent signal integration. For **FLU** and **EFA**, the best spectral situation is obtained at 297 and 300 K, respectively.

A more intriguing effect is observed in the case of scalemic samples of **EFA** (*e.g.* *ee*(*S*) = 90.5%) where ^{19}F-RCSA and (^{19}F–^{19}F)-RDC evolve differently from one enantiomer to another with respect to the temperature. While $|T_{FF}(S)|$ (major enantiomer) increases linearly with this parameter, as observed in the racemic sample, the evolution of $|T_{FF}(R)|$ is more complex with a drop close to zero Hz at 310 K before increasing again at higher temperatures (see Fig. 6). Fundamentally, this non-linear variation suggests a modification of the average orientation of the (*R*)-isomer within the liquid-crystalline phase, leading to a change in enantiomeric discrimination. In addition to this enantiospecific variation of (^{19}F–^{19}F)-RDC, the ^{19}F $\delta_{aniso}(S)$ and ^{19}F $\delta_{aniso}(R)$ evolve linearly with the temperature, but at different rates resulting in ^{19}F $|\Delta\delta_{aniso}(R, S)|$ = 0.116 ppm at 300 K *versus* 0.099 ppm at 320 K.

Overall, these results highlight the significant impact of solute concentration, enantiomeric ratio and temperature on the enantiomeric resolution of these ^{19}F NMR experiments in lyotropic chiral liquid crystals.

Measurements of enantiomeric excesses and analytical performance on APIs

The determination of enantiopurity of APIs by NMR is a major analytical challenge based on the *ee*% measurement that is by essence a quantitative measurement. Understanding and mastering all the potential experimental biases deserve therefore a real attention. For instance, it is well known that the repetition time (T_R) between successive scans should be long enough to prevent a partial saturation between the targeted analytes. When anisotropic ^{19}F–{^{1}H} NMR is concerned, it is usually addressed by fixing this duration at five times the longer T_1^{aniso} (^{19}F) measured at the expense of the experimental duration and/or signal-to-noise ratio (SNR).

Another possible bias may occur when ^{1}H-decoupling in the heteronuclear experience is applied and leads to a differential nuclear Overhauser effect (nOe) between analytes. To limit this effect, it is recommended to apply the ^{1}H decoupling only during the ^{19}F signal detection period ("inverse gated" experi-

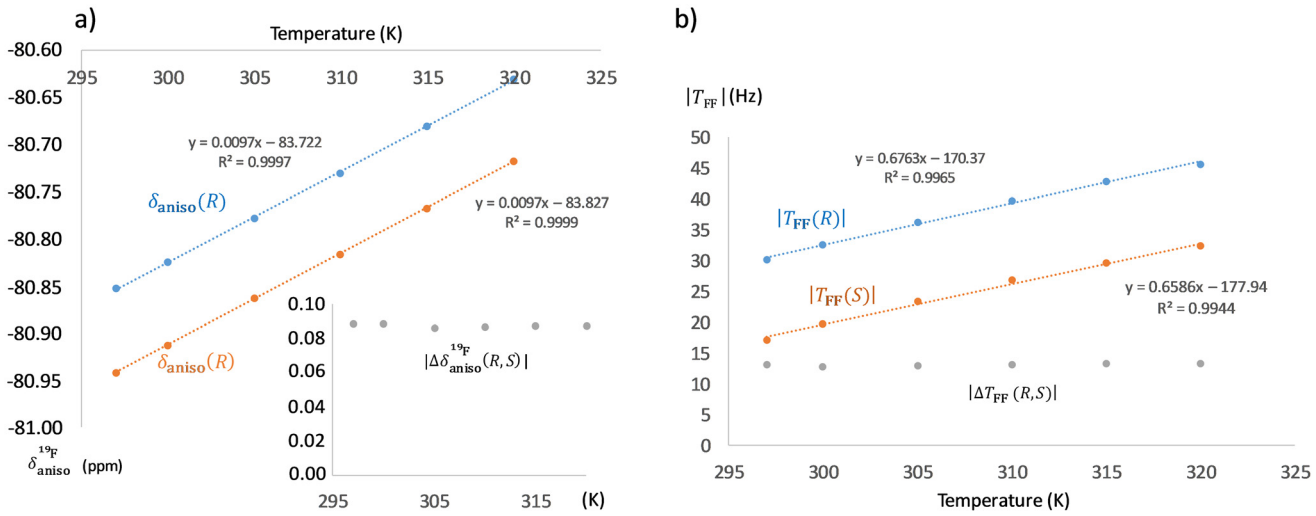

Fig. 5 (a and b) Effect of the temperature on ^{19}F-RCSA and (^{19}F–^{19}F)-RDC evaluated on a 20 mg racemic sample of **EFA** dissolved in PBLG/$CHCl_3$, respectively. These anisotropic observables experience a linear variation with similar slopes between the two enantiomers resulting in no variation of ^{19}F $|\Delta\delta_{aniso}(R, S)|$ and $|\Delta T_{FF}(R, S)|$ in this range of temperatures.

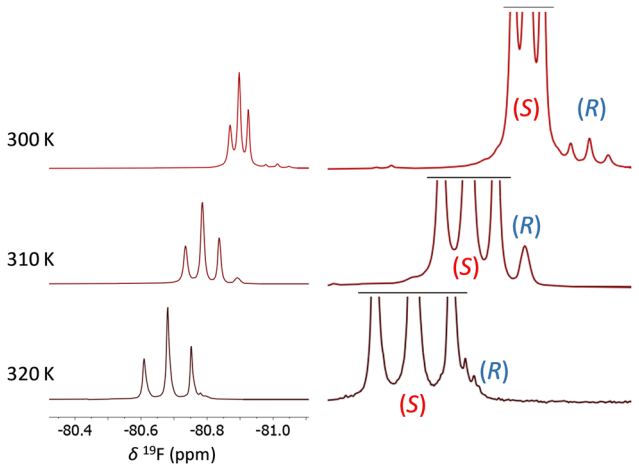

Fig. 6 Effect of the temperature monitored on a 30 mg scalemic sample of **EFA** (*ee*(*S*) = 90.5%) dissolved in PBLG/$CHCl_3$. In contrast to the racemic series, different evolutions of ^{19}F-RCSA and (^{19}F–^{19}F)-RDC are observed from one enantiomer to another leading to variations of signal patterns. The variation of both anisotropic parameters is given in Table SI-3.†

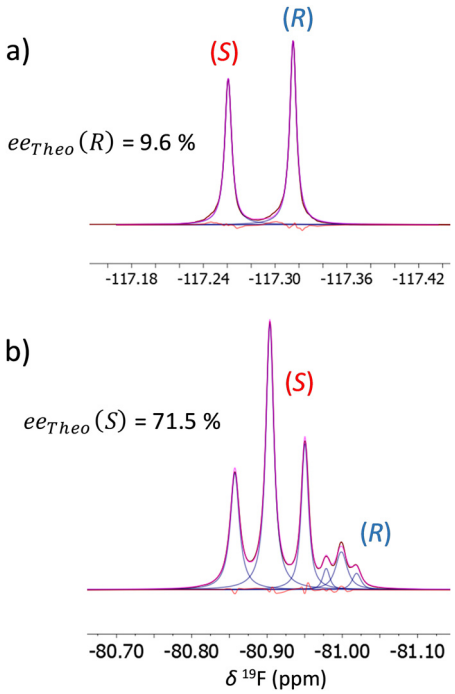

Fig. 7 Examples of 282.4 MHz ^{19}F–{^{1}H} spectra (NS = 8) of scalemic samples of **FLU** (a) and **EFA** (b) in PBLG/$CHCl_3$ at 300 K after line-fitting procedure. Both samples contain a total content of 30 mg of analyte. The reconstructed spectrum (pink line) is well superposed to the experimental one (brown line) leading to an almost flat residue curve (red line). The individual signal components (blue lines) can be extracted for computing the experimental value of *ee*%.

ment). However, these two usual requirements may be alleviated in the case of relative quantification of enantiomers. Indeed, relaxation properties are similar between the two enantiomers and no significant differences of relaxation times have been so far reported in lyotropic liquid crystals, at the best of our knowledge. $T_1^{aniso}(^{19}F)$ have been determined for the *R* and *S*-isomers of both **FLU** ($T_1^{aniso}(^{19}F)$ = 1.2 s) and **EFA** ($T_1^{aniso}(^{19}F)$ = 0.5 s) by the inversion–recuperation method and no differences (greater than the fitting error) have ever been observed between enantiomers. This allows to work with a smaller repetition time ($T_R \approx 1.25 \times T_1^{aniso}(^{19}F)$) which provides the optimal SNR per time unit without a systematic quantitative bias. Interestingly, this condition therefore improves the method's detection limit for a given experimental duration.

^{19}F–{^{1}H} NMR experiments (NS = 8, *i.e.* $T_{exp} \approx 10$ s) were carried out on both racemic and scalemic series to evaluate the accuracy of enantiomeric excess measurements in different spectral situations. The experimental *ee*% are derived as in eqn (7) and the signal integration is performed by a line-fitting procedure (see Fig. 7) as described in the Experimental section. The deviation from the expected values of the measurements (*i.e.*, the trueness) is assessed on racemic samples since the expected *ee* = 0% does not suffer from potential weighting uncertainties during the sample preparation. The precision (here defined as short term repeatability) is evaluated by the standard deviation (SD%) computed on series of at least seven successive NMR experiments. Scalemic samples are also considered to evaluate the performance of the method on more challenging cases, such as *ee* ≈ 90%, where large differences of signal area between lines imperfectly resolved are detrimental for an accurate *ee*% determination.

In the case of **FLU** (see Table 2), the trueness evaluated on the racemic sample is lower than 1% (0.8%), which validates

Table 2 Enantiomeric excess determination on a series of **FLU** samples in PBLG/$CHCl_3$ with an increasing *ee*(*R*)[a]

$ee_{Theo.}(R)$[b] (%)	$ee_{Exp.}(R)$[c] (%)	Deviation[d] (%)	SD[e] (%)	SNR (*S*)	SNR (*R*)
0.0	0.8	0.8	0.32	1854	1839
9.6 ± 0.7	9.5	−0.1	0.40	1691	2130
58.2 ± 0.8	57.3	−0.9	0.22	891	3019
88.7 ± 1.1	84.5	−4.2	0.23	337	3465

[a] The total mass of API is nearby 30 mg in all samples. Measurements are achieved by ^{19}F–{^{1}H} NMR experiment of ≈10 s (NS = 8) at 7.05 T (ν_0 = 282.4 MHz). [b] Values given with 95% confidence intervals due to weighing uncertainties for scalemic samples. [c] Mean value of seven successive experiments. [d] Computed as $ee_{Exp} - ee_{Theo}$. [e] Standard deviation computed on seven successive experiments.

the absence of significant biases from partial saturation ($T_R \approx 1.25 \times T_1(^{19}F)$) whenever a trueness of 1% is targeted. The SNR achieved under these experimental conditions ($T_{exp} \approx 10$ s) is of the order of 10^3 and remains higher than 300 even for the minor enantiomer at *ee* = 88.7%. The resulting precision (*i.e.*, SD%) is better than 0.5% for all the **FLU** samples (see Table 2). It could also be noted that precision is not affected by the *ee*% to be measured, which suggests that the uncertainty mainly relies on the line-fitting procedure, rather than a lack of SNR for the minor enantiomer. For scalemic samples, the trueness

remains lower than 1% until $ee(R)$ = 58.2%, but increasing significantly at $ee(R)$ = 88.7% where a deviation of −4.2% is observed. This deviation can arise from an imperfect Lorentzian lineshape of experimental signals causing weak line-fitting errors, which become detrimental for the trueness at very high *ee*%, whenever enantiomeric signals are not perfectly baseline-separated. In the case of **EFA** (see Table 3), the trueness evaluated on the racemic sample is better than 0.5%, which demonstrates again the absence of biases of the proposed method. This good performance is also extended in the case of scalemic samples since the measured values of *ee*% lie in the acceptable interval with deviation lower than 0.5% from the expected values. Table 3 also gives the SNR values associated with the (*R*)- and (*S*)-isomers for a racemic and two scalemic samples of **EFA**. Such fast ^{19}F NMR experiments enable a minimal SNR value of about 200 for the minor *R*-isomer in a sample with $ee(S)$ = 90.5%. This leads to standard deviations lower than 0.5%, even at the highest enantiomeric excess (*i.e.*, $ee(S)$ = 90.5%) highlighting the high precision of this fast ^{19}F NMR method.

Limit of detection of this ^{19}F NMR method. The limits of detection (LOD) of this method ($T_{exp} \approx 10$ s at 7.05 T) have been evaluated for these two APIs. Calculations lead to 42 μg mL^{-1}, *i.e.*, 0.17 μmol mL^{-1} for **FLU**, and 50 μg mL^{-1}, *i.e.*, 0.16 μmol mL^{-1} for **EFA** ^{19}F–{^{1}H} spectra recorded at such concentrations in API are available in Fig. SI-4 and SI-5.† In molar units, LOD values of **EFA** and **FLU** are similar (0.16 μmol mL^{-1} *versus* 0.17 μmol mL^{-1}), despite a difference in molecular weight. This is due to the gain of 3/2 in SNR (measurements made on the central resonance of the triplet) offered by a CF_3 group (three isochronous nuclei distributed over the three lines of a triplet) compared to a monofluorinated site, which counterbalances the higher molecular weight of **EFA** (315.7 *versus* 244.3 g mol^{-1}). To provide an overview of the sensitivity of this ^{19}F–{^{1}H} NMR method under different experimental conditions, the measured values of LOD can be extrapolated using the equation below:

$$SNR \propto N\gamma_e\gamma_d^{3/2}B_0^{3/2}\sqrt{NS} \quad (10)$$

where N is the number of nuclei, γ_e and γ_d are respectively the gyromagnetic ratios of the excited and detected nuclei, B_0 the external magnetic field and NS the number of accumulated scans. Fig. 8a presents the estimated LOD at different magnetic field strengths B_0 for two fixed experimental durations T_{exp} (10 s and 120 s) while Fig. 8b shows the evolution of LOD as a function of T_{exp} for two given B_0 values (7.05 and 9.41 T). The black crosses seen on the graphs point out the experimental LOD value of 0.16 μmol mL^{-1} obtained for **EFA** in this study ($T_{exp} \approx 10$ s at 7.05 T).

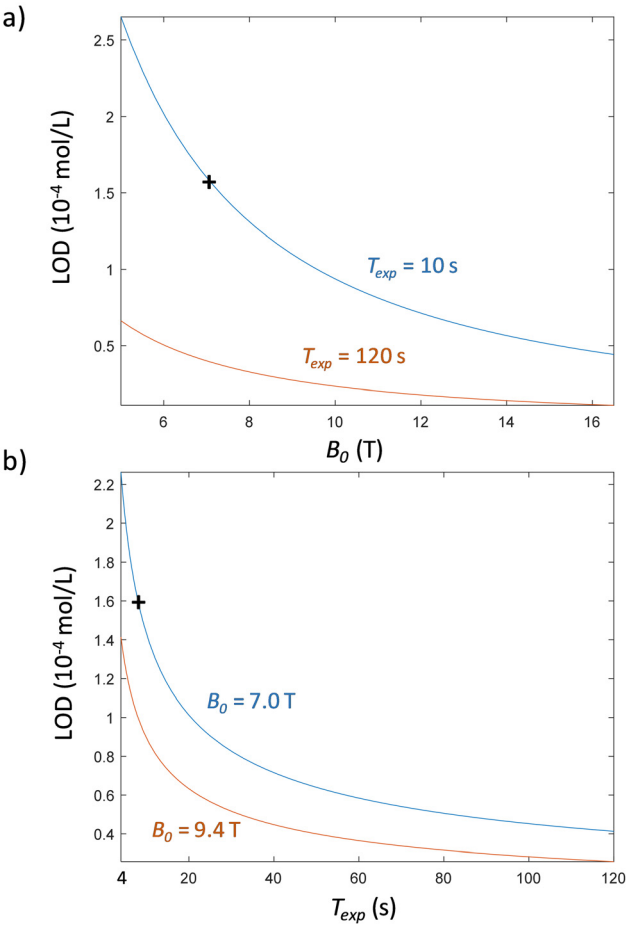

Fig. 8 Estimated LOD according to the magnetic field B_0 of the spectrometer with fixed experimental durations T_{exp} (a) and as a function of T_{exp} for given B_0 values (b). The LOD curves are extrapolated *via* eqn (10) from the experimental LOD of **EFA** (black cross).

Table 3 Enantiomeric excess determination on a series of **EFA** samples in PBLG/$CHCl_3$ with an increasing $ee(S)$[a]

$ee_{Theo.}(S)$[b] (%)	$ee_{Exp.}(S)$[c] (%)	Deviation[d] (%)	SD[e] (%)	SNR (*S*)	SNR (*R*)
0.0	−0.4	−0.4	0.37	1762	1743
71.5 ± 0.9	71.7	0.2	0.50	2816	517
90.5 ± 1.1	90.9	0.4	0.35	3686	191

The footnotes (*a*–*e*) are identical to footnotes of Table 2.

Conclusion

Proposing new, effective and reliable tools for the analysis of active pharmaceutical ingredients is one of today's challenges for the research academic laboratories and pharmaceutical industrial ones, with major societal implications for human health. In this work, we have assessed, for the first time, the analytical potential of ^{19}F NMR in lyotropic PBLG-based CLCs to determine enantiomeric excesses on two (patented) chiral drugs (mono- and polyfluororinated) in pharmacopeia, Efavirenz and Flurbiprofen, using a routine NMR equipment.

Results in terms of spectral enantiodiscriminations are very promising with potential applications in pharmaceutical

analytical laboratories. First, the determination of the *ee*% is obtained with a precision better than 0.5% and a trueness better than 1% (at the exception of one sample) in a high-throughput context (experimental durations ≤ 10 s) and routine NMR setup operating at moderate magnetic fields (*e.g.*, 7.05 T, conventional NMR probe) with a limit of detection of 42 μg mL^{-1} (*i.e.*, 0.17 μmol mL^{-1}) for **FLU**, and 50 μg mL^{-1} (*i.e.*, 0.16 μmol mL^{-1}) for **EFA**, in such experimental conditions. Second, the use of anisotropic NMR interactions such as the ^{19}F–^{19}F residual dipolar couplings of methyl groups, whose amplitude is not related to the magnetic field strength, eases the method transfer at lower magnetic fields. This aspect could make enantiomeric analysis with benchtop NMR spectrometers possible in the near future.

This first study on API has also explored the significant role of the liquid crystal composition, especially the chiral analyte concentration on the resulting ^{19}F-RCSA and (^{19}F–^{19}F)-RDC values, and showing higher values of ^{19}F anisotropic observables on diluted samples as well as variations of the enantiomeric discrimination according to the *ee*%. The analysis of the effect of temperature indicates a slight improvement of the spectral discrimination of enantiomers of **FLU** at 297 K compared to higher temperatures whereas this parameter should be adjusted to avoid detrimental peak-overlaps in the case of **EFA**. The whole understanding of the complex interplay between mesophase composition and sample temperature on the average orientation of analyte and discrimination mechanisms, and thus on the measured residual anisotropic observables, is still an on-going challenge under investigation.

Author contributions

All authors contributed equally to this work. The manuscript was written through contributions of all authors. All authors have given approval to the final version of the manuscript.

Conflicts of interest

The authors declare no conflict of interest.

Acknowledgements

The authors thank Paris-Saclay University and CNRS for their recurrent funding as well as the Ile-de-France region for the SESAME "CRYOMORPHOSE 2022" grant to upgrade NMR equipment of ICMMO's scientific plateform. This work was supported in part by the French National Research Agency: ANR INENDRA project, grant ANR-23-CE29-0005-01, from November 2023. They also acknowledge Valentin Henriet and Benoit Kuate-Wafo who participated to this projet during their internship. Finally, we would like to thank the referees for their comments and suggestions.

References

1 B. S. Sekhon, *J. Mod. Med. Chem.*, 2013, **1**, 10–36.
2 E. Sanganyado, Z. Lu, Q. Fu, D. Schlenk and J. Gan, *Water Res.*, 2017, **124**, 527–542.
3 W. H. Brooks, W. C. Guida and K. G. Daniel, *Curr. Top. Med. Chem.*, 2011, **11**, 760–770.
4 A. Calcaterra and I. D'Acquarica, *J. Pharm. Biomed. Anal.*, 2018, **147**, 323–340.
5 E. L. Izake, *J. Pharm. Sci.*, 2007, **96**, 1659–1676.
6 M. Thunhorst and U. Holzgrabe, *Magn. Reson. Chem.*, 1998, **36**, 211–216.
7 M. Shamsipur, L. S. Dastjerdi, S. Haghgoo, D. Armspach, D. Matt and H. Y. Aboul-Enein, *Anal. Chim. Acta*, 2007, **601**, 130–138.
8 M. Pérez-Trujillo and A. Virgili, *Tetrahedron: Asymmetry*, 2006, **17**, 2842–2846.
9 P. Borowiecki, *Tetrahedron: Asymmetry*, 2015, **26**, 16–23.
10 J. Redondo, A. Capdevila and S. Ciudad, *Chirality*, 2013, **25**, 780–786.
11 T. Wang, Q. Liu, M. Wang, J. Zhou, M. Yang, G. Chen, F. Tang, E. Hatzakis and L. Zhang, *Anal. Chem.*, 2020, **92**, 3636–3642.
12 V. K. Vashistha and R. Bhushan, *Tetrahedron: Asymmetry*, 2015, **26**, 304–311.
13 R. N. Rao and K. Santhakumar, *New J. Chem.*, 2016, **40**, 8408–8417.
14 T. J. Wenzel, in *Stereoselective Synthesis of Drugs and Natural Products*, ed. V. Andrushko and N. Andrushko, John Wiley & Sons, Inc., Hoboken, NJ, USA, 2013, pp. 1–24.
15 T. J. Wenzel and J. D. Wilcox, *Chirality*, 2003, **15**, 256–270.
16 D. Parker, *Chem. Rev.*, 1991, **91**, 1441–1457.
17 T. R. Hoye, C. S. Jeffrey and F. Shao, *Nat. Protoc.*, 2007, **2**, 2451–2458.
18 S. Jang and H. Kim, *Org. Lett.*, 2020, **22**, 4185–4189.
19 L.-P. Li and B.-H. Ye, *Inorg. Chem.*, 2017, **56**, 10717–10723.
20 M. D. McCreary, D. W. Lewis, D. L. Wernick and G. M. Whitesides, *J. Am. Chem. Soc.*, 1974, **96**, 1038–1054.
21 L. Zhang, A. F. Martins, P. Zhao, M. Tieu, D. Esteban-Gómez, G. T. McCandless, C. Platas-Iglesias and A. D. Sherry, *J. Am. Chem. Soc.*, 2017, **139**, 17431–17437.
22 H. Dodziuk, W. Koźmiński and A. Ejchart, *Chirality*, 2004, **16**, 90–105.
23 S. Jang and H. Kim, *Org. Lett.*, 2020, **22**, 7804–7808.
24 B. Huang, L. Xu, N. Wang, J. Ying, Y. Zhao and S. Huang, *Anal. Chem.*, 2022, **94**, 1867–1873.
25 L. Xu, Q. Wang, Y. Liu, S. Fu, Y. Zhao, S. Huang and B. Huang, *Analyst*, 2023, **148**, 4548–4556.
26 B. Huang, L. Xu, J. Ying, Y. Zhao and S. Huang, *Anal. Chim. Acta*, 2022, **1230**, 340402.
27 G. Gu, C. Zhao, W. Zhang, J. Weng, Z. Xu, J. Wu, Y. Xie, X. He and Y. Zhao, *Anal. Chem.*, 2024, **96**, 730–736.
28 A. Saupe and G. Englert, *Phys. Rev. Lett.*, 1963, **11**, 462–464.
29 P. Lesot, C. Aroulanda, P. Berdagué, A. Meddour, D. Merlet, J. Farjon, N. Giraud and O. Lafon, *Prog. Nucl. Magn. Reson. Spectrosc.*, 2020, **116**, 85–154.

30 C. Aroulanda and P. Lesot, *Chirality*, 2022, **34**, 182–244.
31 B. Luy, *J. Indian Inst. Sci.*, 2010, **90**, 119–132.
32 P. Tzvetkova, B. Luy and S. Simova, *Topics in chemistry and material science*, 2011, vol. 5, pp. 70–77.
33 P. Lesot, P. Berdagué, A. Meddour, A. Kreiter, M. Noll and M. Reggelin, *ChemPlusChem*, 2019, **84**, 144–153.
34 G. W. Li, X.-J. Wang, S.-H. Shi, L.-T. Liu, J.-Q. Li, H. Sun, Z.-Q. Wu and X. Lei, *Anal. Chem.*, 2023, **95**, 18850–18858.
35 P. Berdagué, J.-E. Herbert-Pucheta, V. Jha, A. Panossian, F. R. Leroux and P. Lesot, *New J. Chem.*, 2015, **39**, 9504–9517.
36 M. Inoue, Y. Sumii and N. Shibata, *ACS Omega*, 2020, **5**, 10633–10640.
37 M. Jakubcova, A. Meddour, J.-M. Péchiné, A. Baklouti and J. Courtieu, *J. Fluor. Chem.*, 1997, **86**, 149–153.
38 V. Madiot, P. Lesot, D. Grée, J. Courtieu and R. Grée, *Chem. Commun.*, 2000, 169–170.
39 A. R. Phillips and G. J. Sharman, *Chem. Commun.*, 2004, 1330–1331.
40 N. M. Davies, *Clin. Pharmacokinet.*, 1995, **28**, 100–114.
41 V. Namasivayam, M. Vanangamudi, V. G. Kramer, S. Kurup, P. Zhan, X. Liu, J. Kongsted and S. N. Byrareddy, *J. Med. Chem.*, 2019, **62**, 4851–4883.
42 M. E. D. Pietro, C. Aroulanda, G. Celebre, D. Merlet and G. D. Luca, *New J. Chem.*, 2015, **39**, 9086–9097.
43 P. Trigo-Mouriño, C. Merle, M. R. M. Koos, B. Luy and R. R. Gil, *Chem. – Eur. J.*, 2013, **19**, 7013–7019.
44 R. Ferrazza, B. Rossi and G. Guella, *J. Phys. Chem. B*, 2014, **118**, 7147–7155.
45 A. Pérez, D. de Saá, A. Ballesteros, J. L. Serrano, T. Sierra and P. Romero, *Chem. – Eur. J.*, 2013, **19**, 10271–10279.